


How do T Tauri stars accrete?

Lee Hartmann¹, Jaehan Bae¹ 

¹*Department of Astronomy, University of Michigan, 1085 S. University Ave, Ann Arbor, MI 48105, USA*

Accepted XXX. Received YYY; in original form ZZZ

ABSTRACT

We conjecture that observed protoplanetary disc accretion rates may be explained with low viscosities which could be the result of hydrodynamic turbulence. We show that viscosities parameterized in the usual way with $\alpha \gtrsim 10^{-4}$, comparable to values suggested for hydrodynamic turbulence, can explain the observed accretion rates and lifetimes with plausible inner disc surface densities. Our models are also in better agreement with surface density estimates of the minimum mass solar nebula than models with rapid transport for a given mass accretion rate, such as recent models of accretion driven by magnetic winds. The required surface densities are a natural result of the protostellar infall phase, as long as non-gravitational transport is limited. We argue that, in addition to possible non-ideal magnetic transport due to disc winds possibly modified by the Hall effect, the effects of low-viscosity hydrodynamic accretion deserve more consideration.

Key words: accretion, accretion discs – protoplanetary discs

1 INTRODUCTION

T Tauri stars accrete significant amounts of gas over typical timescales of a few Myr, but it has proved difficult to identify precisely why they do so. It was recognized early on that the magnetorotational instability (MRI), which provides a satisfactory explanation for turbulent transport in ionized astrophysical discs (Balbus & Hawley 1998), was unlikely to be effective in large regions of cold protoplanetary discs. To explain the observed mass accretion in T Tauri stars, Gammie (1996) proposed that cosmic rays could sufficiently ionize upper disc layers for the MRI to operate, leaving a non-turbulent, non-accreting “dead zone” sandwiched in between. However, Gammie’s model included only Ohmic dissipation; recent numerical simulations indicate that ambipolar diffusion quite effectively quenches the MRI over large regions of discs (e.g., Bai & Stone 2013; Bai 2014; Gressel et al. 2015; Simon et al. 2015), and any reduction of cosmic ray ionizing fluxes by disc winds would make MRI activation even less likely Cleeves et al. (2015) (although there may be some MRI activation in the outermost regions; Simon et al. 2015).

Observations suggesting low turbulence in protoplanetary discs also limit the possible levels of MRI turbulence. Flaherty et al. (2015) analyzed line profiles of differing isotopologues of CO to place low limits on turbulent velocities in the outer disc of HD 163296. More indirectly, low turbulence is needed for models in which dust concentration in pressure maxima explain observations of narrow

rings, gaps, and possibly vortex structures (Zhu & Baruteau 2016; Bae et al. 2017; Dong et al. 2017). Finally, several recent studies have found no evidence for the correlations between disk masses, sizes, and accretion rates expected for strongly-viscous disks (Rafikov 2017; Tazzari et al. 2017; Lodato et al. 2017).

The time-dependent non-ideal MHD disc simulations which demonstrated the ineffectiveness of the MRI in regions where ambipolar diffusion is important instead found strong disc winds which drive accretion in narrow upper disc layers (Bai 2014, 2015; Gressel et al. 2015), echoing the pioneering study of Königl (1989). Bai (2016) has developed one of the most complete pictures of how winds can drive the necessary accretion in protoplanetary discs, updating earlier ideas Pudritz & Norman (1983); Ferreira & Pelletier (1993); Ferreira et al. (2006). The Hall effect in protoplanetary discs may also modify this picture (e.g., Salmeron & Wardle 2008), as it is capable of producing strong laminar stresses if the magnetic field and angular momentum vector are aligned, or intermittent turbulent stresses in the anti-aligned case (Lesur et al. 2014; Simon et al. 2015; Béthune et al. 2017; Bai & Stone 2017).

However, the effectiveness of non-ideal magnetic transport depends on uncertain or unknown parameters, such as the exact levels of ionization in upper disc layers and magnetic field strengths (e.g., Armitage et al. 2013). The amount of magnetic flux dragged in from the protostellar cloud and retained in the disc must be regarded as uncertain (Guilet & Ogilvie 2014; Okuzumi et al. 2014; Bai & Stone 2017), especially as there are no direct in situ constraints,

* E-mail: lhartm@umich.edu

and because magnetic flux loss via ambipolar diffusion as the protostellar envelope collapses is likely to be very important, if not essential, to forming discs of the observed ~ 100 AU sizes (Masson et al. 2016).

Observational evidence in favor of the magnetic models is limited. While the jets and winds from inner discs almost certainly require magnetic acceleration (e.g., Ferreira et al. 2006), these may actually arise from warmer regions where the MRI can operate. There is evidence for slower outer disc winds in the form of low-velocity forbidden line emission (Pascucci et al. 2011; Rigliaco et al. 2013), but it isn't clear whether these flows might be entirely the result of photoevaporatively-driven mass loss with minimal or no magnetic coupling (Simon et al. 2016). Finally, the bimodality of the Hall effect depending upon the alignment of poloidal field and angular momentum, or other distinct differences such as quenching accretion, one-sided winds, etc. seen in the simulations of Béthune et al. (2017) currently do not have obvious observational support (see also Bai & Stone 2017).

In view of the likely weak coupling between magnetic fields (if any) and gas in much of protoplanetary discs, increased attention has been paid to hydrodynamic sources of turbulence (see Fromang & Lesur 2017, for a review), such as the vertical shear instability (VSI; Urpin 2003; Nelson et al. 2013; Lin & Youdin 2015) convective overstability (Klahr & Hubbard 2014), the “zombie vortex” instability (Marcus et al. 2015; but see Lesur & Latter 2016), or even turbulence driven by planets (Bae et al. 2016; Fung & Chiang 2017). While these instabilities can in principle produce angular momentum transport, the levels of viscosity produced are so low that accretion during T Tauri lifetimes could only come from inner regions of discs; viscous transport timescales at large radii are too long compared with observed disc lifetimes. Conventional disc mass estimates suggest that the needed reservoir to maintain disc accretion over typical lifetimes must extend to the outer disc (§2). However, disc masses derived from mm- and sub-mm wave dust emission are sensitive to uncertain dust opacities, and inner disc dust is generally thought to be optically thick at these wavelengths (§4), thus providing no observational constraints.

In this paper we explore the possibility that protoplanetary disc (T Tauri) accretion can be explained with low turbulent viscosities potentially achievable by a variety of hydrodynamic instabilities. Fung & Chiang (2017) made the suggestion that turbulence driven by a series of super-Earths in inviscid discs could explain the observed accretion rates of $\gtrsim 10^{-8} M_{\odot} \text{ yr}^{-1}$; here we consider the more general situation of weak viscous transport, regardless of its origin. We show that plausible inner disc masses can provide the needed reservoirs of material, such that the observed accretion can be explained by a combination of low-viscosity, potentially purely hydrodynamic, turbulence and thermal MRI activation in the warm, innermost disc.

2 MASS RESERVOIRS NEEDED FOR ACCRETION

The durations and rates of accretion in T Tauri stars place statistical constraints on the minimum amount of gas ini-

tially present in their discs. The most reliable measures of mass accretion rates come from excess optical emission produced as gas funnels in along magnetospheric flux tubes and shocks at the stellar photosphere (e.g., Hartmann et al. 2006). A recent analysis of accretion rate estimates by G. Herczeg (presented in Hartmann et al. 2016) found a mean dependence of the mass accretion rate on stellar mass of

$$\dot{M} = 10^{-7.9} M_{*}^{2.1} M_{\odot} \text{ yr}^{-1}, \quad (1)$$

where the stellar mass M_{*} is measured in solar masses. Removing this mass dependence for stars with masses between 0.3 and $1.0 M_{\odot}$ yields a time dependence $\dot{M} \propto t^{-1.07}$. Given the large observed scatter about these trends, we simplify Herczeg's results in this paper to

$$\dot{M} = 1.8 \times 10^{-8} M_{0.7}^2 t_6^{-1} M_{\odot} \text{ yr}^{-1}, \quad (2)$$

where t_6 is the age in units of Myr. The total mass accreted between times t_0 and t_f is then

$$M_{acc} = 1.8 \times 10^{-2} M_{0.7}^2 \ln(t_f/t_0) M_{\odot}. \quad (3)$$

As this relation was derived for optically-visible young stars, we take t_0 to be the time when infall to the disc has ceased (i.e., after the protostellar phase). Kenyon & Hartmann (1995) suggested that the protostellar phase lasts between 0.1 - 0.2 Myr, while the more recent and complete study by Evans et al. (2009) estimated protostellar lifetimes ~ 0.5 Myr. Here we adopt a compromise value of $t_0 \sim 0.4$ Myr, consistent with the fits being derived mostly from stars with larger ages. The fraction of accreting stars decreases steadily with increasing age, such that only about 50% of all stars show significant accretion at ages of 3 Myr, with a much smaller fraction lasting for 10 Myr (Hernández et al. 2007); the e-folding time for near-infrared excesses or measurable accretion to disappear is estimated to be $\sim 2.3 - 3.0$ Myr (Fedele et al. 2010). We therefore set $t_f = 3$ Myr, and find an estimated average accreted mass during the T Tauri phase of

$$\langle M_{acc} \rangle \approx 0.036 M_{0.7}^2 M_{\odot}. \quad (4)$$

To compare with observational estimates of disc masses from dust emission, we suppose that a typical T Tauri star has an age of ~ 2 Myr, and adopt an e-folding time for the end of accretion = 3 Myr as above. Then the typical accretion rate for the fiducial stellar mass of $M_{*} = 0.7 M_{\odot}$ is $\sim 0.9 \times 10^{-8} M_{\odot} \text{ yr}^{-1}$ and the mass that will be accreted later is $\sim 0.01 M_{\odot}$. While this is in reasonable agreement with the median disc mass $\sim 0.005 M_{\odot}$ estimated from mm-wave dust emission of stars in the Taurus molecular cloud (e.g., Williams & Cieza 2011), it must be emphasized that this is the accreted mass, and the disc masses must be larger if there is to be anything left to form planets.

Although the scatter around the mean values for accretion and mass reservoirs given in equations 2 and 4 is large, these results are important in that infall onto the star traces the bulk gas, in contrast to estimates from dust emission which are sensitive to the size distributions of the solids and which do not trace mass in optically-thick regions. Williams & Best (2014) attempted to determine gas masses by analyzing the emission from CO isotopologues, but their results yielded masses an order of magnitude too small to account for the reservoir of mass needed to sustain accretion, and thus are probably strongly biased by CO freeze-out onto grains or incorporation into other bodies.

3 RAPID MASS TRANSPORT FROM THE OUTER DISC?

Because the typical mass reservoirs needed for T Tauri accretion are comparable to (or exceed) usual estimates for entire discs, it is usually assumed that mass must be accreted from large radii during T Tauri lifetimes. To fix ideas, we consider a disc around a central star of mass of $0.7M_{\odot}$ and assume a disc temperature distribution $T = 200(R/\text{AU})^{-1/2}$ K, motivated by the radiative transfer models of [D'Alessio et al. \(2001\)](#). We further assume that the disc has a viscosity

$$\nu = \alpha c_s^2 / \Omega, \quad (5)$$

where c_s is the sound speed and Ω is the Keplerian angular velocity. Then the viscous timescale as a function of radius is then

$$t_{\nu} \sim \frac{R^2}{\nu} = 1.2 \times 10^4 \alpha_{-2}^{-1} T_{200}^{-1} M_{0.7}^{-1/2} \frac{R}{\text{AU}} \text{yr}, \quad (6)$$

where $\alpha_{-2} = \alpha/0.01$ and T_{200} is the disc temperature at 1 AU in units of 200 K.

Thus, if the mass reservoir for accretion must extend to ~ 100 AU during a T Tauri lifetime of a few Myr, the viscous parameter must be in the range $\alpha \sim 10^{-2} - 10^{-3}$ ([Hartmann et al. 1998](#)). While such viscosities could plausibly be achieved in an MRI-active disc, this is unlikely to be the case for protoplanetary discs (§1). Moreover, there is weak or little empirical evidence for the relations between disc size, mass, and accretion rate predicted by highly viscous disc models ([Rafikov 2017](#); [Tazzari et al. 2017](#); [Lodato et al. 2017](#)).

It is worth noting that high viscosities with typical T Tauri accretion rates are incompatible with estimates of mass surface densities for the lowest mass estimates for the solar nebula (the “minimum-minimum mass solar nebula” (M-MMSN), [Weidenschilling 1977](#); [Hayashi 1981](#)) let alone larger values for the MMSN ([Desch 2007](#)), or estimates of the typical “minimum mass extrasolar nebula” derived assuming in-situ formation of super-Earth systems [Chiang & Laughlin \(2013\)](#). Using the steady state result $\dot{M} = 3\pi\nu\Sigma$ to estimate the surface density at 1 AU given the accretion rate and viscosity parameter,

$$\Sigma_1 \sim 200 \dot{M}_{-8} \alpha_{-2}^{-1} T_{200}^{-1} \text{g cm}^{-2}, \quad (7)$$

where \dot{M}_{-8} is the mass loss rate in units of $10^{-8}M_{\odot} \text{yr}^{-1}$. Thus, to achieve even the M-MMSN surface density of 1700g cm^{-2} implies $\alpha \sim 10^{-3}$ if discs are viscous. While the solar nebula is obviously only one object, the existence of many compact extrasolar planetary systems suggests there may be a need for higher inner disc mass surface densities difficult to achieve with high viscosities.

The relationships between accretion rates and disc surface densities of non-ideal MHD transport models discussed in §1 are not clear, as they are not describable by a turbulent α viscosity; there may be some relation due to the dependence of the stresses on the plasma β . Rapid transport can be consistent in some cases with inner disc surface densities below the M-MMSN (see, for example, [Figure 6 of Bai 2016](#)).

4 SLOW MASS TRANSPORT FROM THE INNER DISC?

Given that mass reservoirs estimated from dust emission are at best barely sufficient to sustain typical accretion, it may seem counter-intuitive to consider whether the inner disc alone can supply the needed mass. However, there are very few observational constraints on inner disc surface densities, both because these regions are still mostly unresolved spatially and the dust emission from the inner disc is expected to be optically thick (see, for example, [Tazzari et al. 2016](#)).¹

To see more quantitatively what is required for adequate accretion at low viscosities, we develop a vertically-integrated disc model with both viscous and irradiation heating. We assume steady accretion in the inner regions, such that the surface density is given by

$$\dot{M} = 3\pi\alpha c_s^2 \Sigma \Omega^{-1}. \quad (8)$$

The sound speed appropriate to the central temperature

$$T_c^4 = T_v^4 + T_i^4, \quad (9)$$

where

$$T_v^4 = \frac{3\tau}{8} \frac{3GM_*\dot{M}}{8\pi\sigma R^3}, \quad (10)$$

where τ is the vertical optical depth from the midplane ([Hubeny 1990](#)).

We use the low temperature dust opacity from [Zhu et al. \(2009\)](#) of $\kappa = 5.3 \times 10^{-2} f T^{0.738} \text{cm}^2 \text{g}^{-1}$ when $T < 1500 \text{K}$, modified by the factor f to account for reductions in opacity due to depletion of small dust which dominates the radiative trapping in the warmer inner regions of the disc. Observations, which provide clear evidence for grain growth in outer discs (e.g., [Tazzari et al. 2016](#)), implies a reduction of the abundance of small grains. More directly, detailed modeling of spectral energy distributions require depletions of small dust in upper disc layers in the range of 10^{-1} to 10^{-3} ([Furlan et al. 2006](#)). We therefore adopt values of $f = 0.1, 0.01$ as observationally justifiable.

We do not model regions where the above equations would yield $T > 1500 \text{K}$; we simply assume the MRI is thermally activated, with a much larger α , and thus adjusts the surface density and temperature to accommodate the mass accreting from the adjacent colder region.

For a given accretion rate, low viscosities imply large surface densities, which can approach values such that transport by gravitational instability (GI) must be considered. Numerical simulations indicate GI-driven spiral waves readjust disc surface densities rapidly such that the Toomre parameter $Q = c_s\Omega/(\pi G\Sigma)$ approaches ≈ 1.4 ([Boley et al. 2006](#)). At somewhat larger values of Q , some transport can still occur with decreasing efficiency, becoming negligible at $Q \geq 2$ ([Kratter et al. 2008](#); [Griv 2006](#)). We therefore limit the surface density such that when equation 8 would imply strong GI transport, we determine the surface density assuming $Q = 2$. This means that the accretion rate in these regions is no longer constant.

¹ Transitional discs (e.g., discs with large inner holes or gaps in dust) have much greater small dust depletions ([Espaillat et al. 2014](#)), but these are clearly quite evolved from their initial conditions.

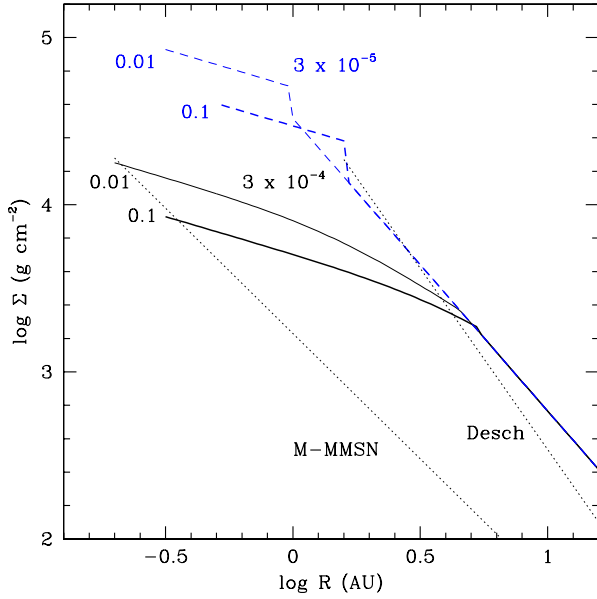


Figure 1. Surface density distributions for discs heated by both viscous dissipation and stellar irradiation, for an inner disc accretion rate of $2 \times 10^{-8} M_{\odot} \text{ yr}^{-1}$. The solid curves are the results for $\alpha = 3 \times 10^{-4}$, with $f = 0.1$ (heavy curve) and $f = 0.01$ (lighter curve). The dashed curves show the surface densities for $\alpha = 3 \times 10^{-5}$, with $f = 0.1$ and 0.01 for the heavy and lighter lines, respectively. The transition to a steeper decrease in Σ at larger radii indicates the regions where the $Q = 2$ GI-limit comes into effect (see text). The jump in surface density is due to the simple way we switch between steady accretion and the GI-limit. The outer dotted line shows the Σ for the MMSN of Desch (2007) while the inner line is the M-MMSN.

Figure 1 shows the surface density distributions for the fiducial $0.7 M_{\odot}$ star with $T_i = 200(R/\text{AU})^{-1}$ K as before, for accretion rates of $\dot{M} = 2 \times 10^{-8} M_{\odot} \text{ yr}^{-1}$, $\alpha = 3 \times 10^{-4}$, 3×10^{-5} , and $f = 0.1, 0.01$. With the larger viscosity parameter, the surface density distribution is consistent with steady accretion out to about 5 AU, while for $\alpha = 3 \times 10^{-5}$ there is only a very narrow region interior to $\sim 1-2$ AU that is in steady state, depending upon f . In general, lower opacities lead to somewhat higher surface densities as the amount of trapping of viscously-generated heat is reduced. In the regions where $Q = 2$ limits the surface density, the accretion rate is no longer constant but decreases with increasing radius. This means that once the inner regions drain, and accretion is sustained from the GI-limited regions, the accretion rate into the central regions should decrease, as we verify in the following section with time-dependent models. The surface densities are well above the M-MMSN but are comfortably below the MMSN of Desch (2007) for $\alpha = 3 \times 10^{-4}$ and even consistent for $\alpha = 3 \times 10^{-5}$.

In Figure 2 we plot the mass interior to the radius R where the viscous timescale is t_{ν} . Both high mass loss rate models show approximately the same mass, $\sim 0.02 M_{\odot}$, within a radius where $t_{\nu} \sim 3$ Myr; although the steady region is smaller at low viscosity, the surface density is higher and the viscous timescales are longer at a given radius. The transition to the $Q = 2$ region is evident from the breaks in the curves. The model mass reservoirs are within a factor

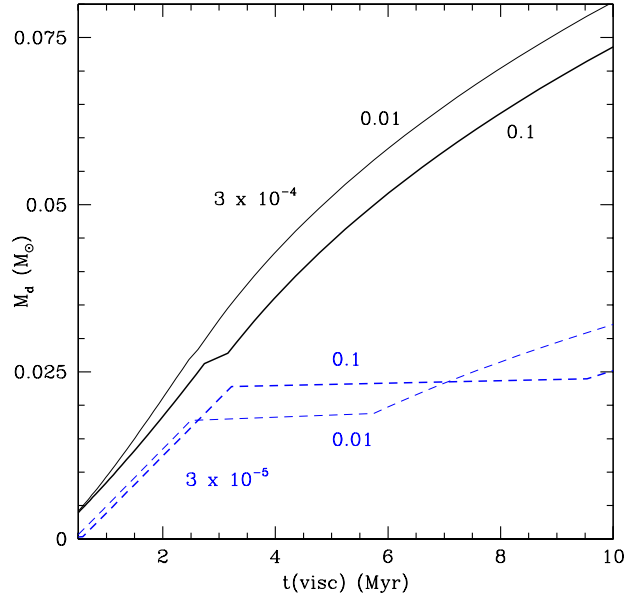


Figure 2. The enclosed mass as a function of the viscous timescale R^2/ν for the model surface densities shown in Figure 1, with the same line types for the different cases.

of two of the observational estimate of equation 4, and thus these simple calculations suggest that the necessary accretion rates can be maintained over timescales ~ 3 Myr.

5 LOW-VISCOSITY DISC EVOLUTION WITH INFALL

Whether T Tauri discs have relatively large inner disc surface densities as shown in Figure 1 depends on initial conditions as well as requiring low viscosities (or other, slow, transport). To explore the possible initial disc mass distribution we employ a simplified version of the methods used in Bae et al. (2013) and Zhu et al. (2010) to follow disc evolution with infall. As in those previous investigations, we use a model of infall to the disc motivated by the Terebey et al. (1984) model for the collapse of a rotating protostellar cloud, but these one-dimensional calculations do not include an active layer. Here, we briefly summarize the time-dependent model with infall; for more details we refer readers to Section 2 of Bae et al. (2013).

We solve the one-dimensional mass and angular momentum conservation equations to evolve the disc surface density, adopting the infall model of Cassen & Moosman (1981) modified as in Bae et al. (2013). The two equations combine into a diffusion equation as

$$\dot{M} = 6\pi R^{1/2} \frac{\partial}{\partial R} (R^{1/2} \Sigma \nu) + \frac{2\pi R^2 \Sigma}{M_R} \frac{\partial M_R}{\partial t} - 4\pi \left(\frac{R}{GM_R} \right)^{1/2} (\Lambda(R, t) - g(R, t) R^2 \Omega(R)), \quad (11)$$

where M_R is the sum of the mass of the central star and the disc within a radius R and Λ and g describe the angular momentum and mass flux per unit distance from the infalling material. In the diffusion equation, the first term represents

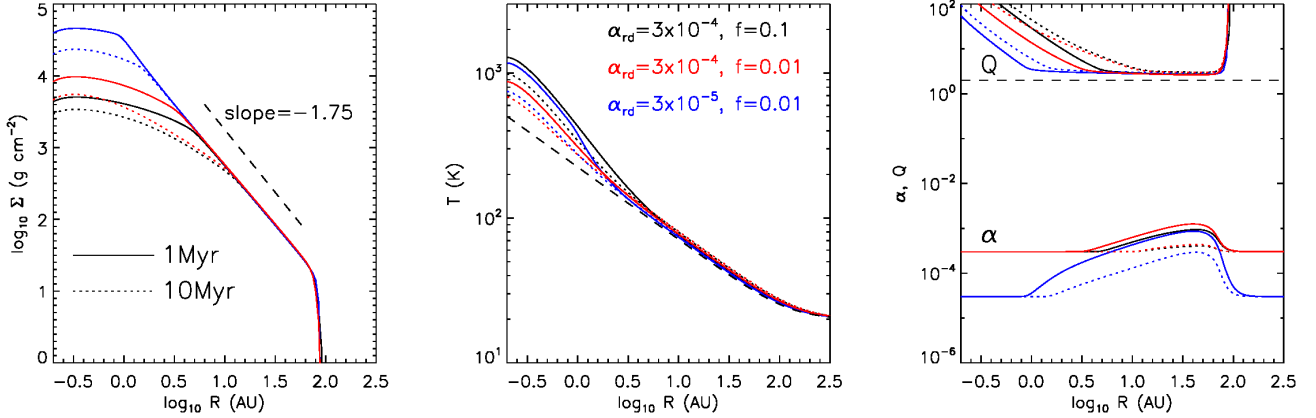


Figure 3. The radial distributions of (left) the surface density, (middle) the temperature, and (right) viscosity parameter α and Toomre Q parameter. In each panel, black curves present results with $\alpha_{\text{rd}} = 3 \times 10^{-4}$ and $f = 0.1$, red curves present results with $\alpha_{\text{rd}} = 3 \times 10^{-4}$ and $f = 0.01$, and blue curves present results with $\alpha_{\text{rd}} = 3 \times 10^{-5}$ and $f = 0.01$, respectively. The solid and dotted curves are radial profiles at 1 and 10 Myr, respectively. In the left panel, the dashed curve indicates a power-law slope of -1.75 . In the middle panel, the dashed curve indicates the external irradiation-dominated temperature for $M_* = 0.7 M_{\odot}$; the excess temperature above this line is due to viscous heating. In the right panel, the dashed curve indicates $Q = 2$.

disc accretion due to viscosity, the second term represents the mass redistribution due to the change in central stellar mass over time, and the third term represents the accretion arising due to the infalling material.

The disc temperature is computed by balancing heating and radiative cooling,

$$C_{\Sigma} \frac{\partial T}{\partial t} = Q_{\text{heat}} - Q_{\text{cool}}, \quad (12)$$

where $C_{\Sigma} = \Sigma c_{\Sigma}^2 / T$ is the heat capacity. The heating term Q_{heat} consists of the viscous heating, the heat generated by the shock dissipation of infalling material, and the external irradiation which includes the stellar luminosity, accretion luminosity, and the heat from the background envelope cloud ($T_{\text{bg}} = 20$ K). The radiative cooling rate Q_{cool} is calculated as

$$Q_{\text{cool}} = \frac{16}{3} \sigma T^4 \frac{\tau}{1 + \tau^2}, \quad (13)$$

where $\tau = f\kappa\Sigma/2$ is the optical depth of the disc and $f\kappa$ is the Rosseland mean opacity used in the previous section for the quasi-steady models.

We implement a total viscosity parameter $\alpha = \alpha_{\text{rd}} + \alpha_{\text{GI}} + \alpha_{\text{MRI}}$, where α_{rd} accounts for any non-GI/MRI transport, which we assume constant at a level 3×10^{-4} or 3×10^{-5} , $\alpha_{\text{GI}} = e^{-Q^2}$ accounts for the transport associated with GI, and α_{MRI} accounts for the transport associated with the MRI, which is set to 0.01 only when the disc temperature exceeds the MRI-activation temperature $T_{\text{MRI}} = 1500$ K.

The calculations start with a $0.1 M_{\odot}$ central protostar surrounded by an $1 M_{\odot}$ cloud. We assume a rigid rotation for the cloud, with a 3% of the breakup angular frequency at the outer cloud edge. Infalling material is added to the disc at a constant rate $\sim 3.4 \times 10^{-6} M_{\odot} \text{ yr}^{-1}$ for ~ 0.24 Myr, forming a $M_* \sim 0.65 M_{\odot}$ star with a $\sim 0.25 M_{\odot}$ of surrounding disc at the end of the infall phase. In this model, most of the stellar mass is accreted during the infall phase through outbursts (see, e.g. Bae et al. 2013; Zhu et al. 2010). The centrifugal radius, marking the outer edge of the disc where matter is

infalling, moves outward with time, reaching ~ 25 AU at the end of the infall phase.

In Figure 3 we present the radial distributions of surface density, temperature, α , and Q at 1 and 10 Myr for the fiducial model with $\alpha_{\text{rd}} = 3 \times 10^{-4}$ and $f = 0.01$. The overall surface density profile is in good agreement with that of the quasi-steady disc model (Figure 1). The disc expands beyond the final infall radius of 25 AU to ~ 100 AU due to the action of gravitational torques, which redistribute material such that the disc has a constant $Q \sim 3$ and thus a power-law density profile $\Sigma \propto R^{-1.75}$ as a result of the $T \propto R^{-1/2}$ temperature distribution in the irradiation-dominated regime. Inward of the Q -limited region, the disc has a roughly constant mass accretion as a function of radius, as assumed in the quasi-steady model. The surface density is flatter because the temperature is dominated by viscous heating, enhanced by radiative trapping due to the large surface density of $\Sigma > 10^3 \text{ g cm}^{-2}$. Note that, without photoevaporation and planet formation, the outer disc surface density remains nearly constant over 10 Myr because of the long viscous timescale for a small viscosity α_{rd} . It is only the inner disc that maintains the accretion onto the central star while the total disc mass is dominated by the outer disc. Thus, the model predicts no relation between disc size, mass, and accretion rate, in agreement with the study of Rafikov (2017).

In Figure 4 we present the mass accretion rate history, along with the total mass accreted onto the central star during the post-infall (T Tauri) phase ($t > 0.24$ Myr). The disc enters a quiescent accretion phase following a number of outbursts after the infall ceases. The accretion rate during the extended quiescent accretion phase starts with $\dot{M} \sim$ a few $\times 10^{-8} M_{\odot} \text{ yr}^{-1}$ and gradually decreases over time. While the magnitude of the accretion rate and the amount of mass accreted ($\sim 0.02 M_{\odot}$ between 1 and 10 Myr) is in reasonable agreement with median observed values, the best fit power-law slope for the $\log t - \log \dot{M}$ relation between 1 and 10 Myr is -0.45 , shallower than the estimated ~ -1 (§2). For this model a faster decrease in accretion rate would have to be explained by photoevaporation or planet formation.

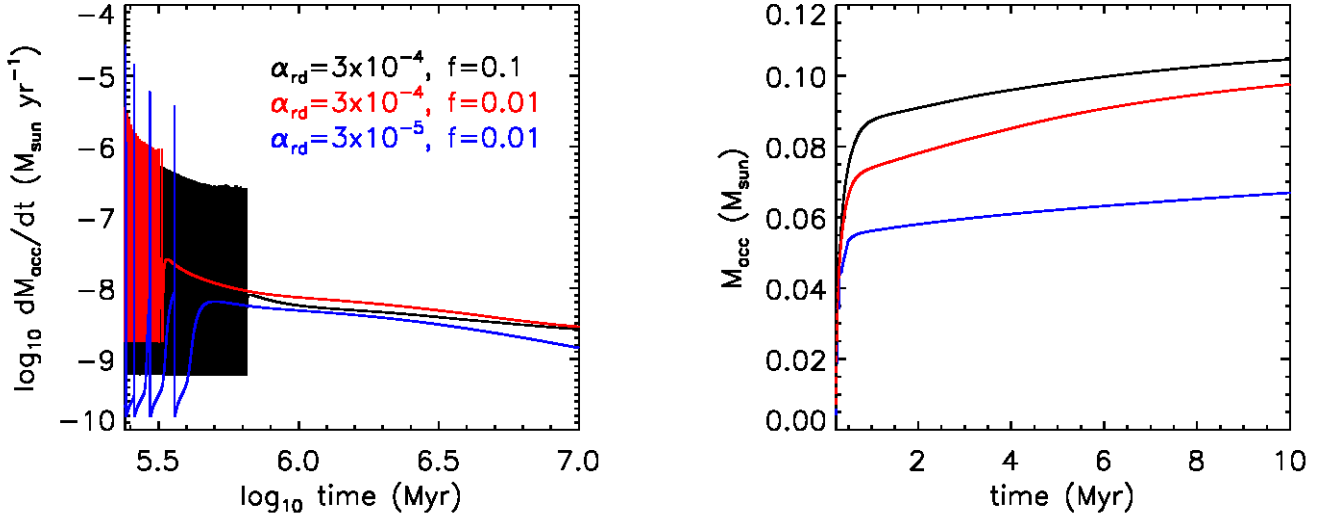


Figure 4. (Left) The accretion rate and (right) total mass accreted as a function of time for (black) $\alpha_{\text{rd}} = 3 \times 10^{-4}$ and $f = 0.1$, (red) $\alpha_{\text{rd}} = 3 \times 10^{-4}$ and $f = 0.01$, and (blue) $\alpha_{\text{rd}} = 3 \times 10^{-5}$ and $f = 0.01$ models. Note that the accreted mass presented here is during the post-infall, T Tauri phase only ($t > 0.24$ Myr).

One effect of our adoption of reduced dust opacities is that it reduces or eliminates the accretion outbursts lasting well through the T Tauri phase seen in our previous simulations (Zhu et al. 2010; Bae et al. 2013), outbursts that are inconsistent with observations. Reducing the opacity reduces or eliminates the T Tauri phase outbursts by reducing the amount of radiative trapping essential to drive temperatures high enough to trigger the MRI. This accounts for the difference in early accretion behavior between the $f = 0.1$ and 0.01 , $\alpha_{\text{rd}} = 3 \times 10^{-4}$ models (left panel of Figure 4), such that larger depletion stops the outbursts sooner. Changing f by a factor of 10 has little effect on the accretion rates because it has only a modest effect on the surface density in the viscous accretion (inner) zone, and no effect on the Q -limited zone where the temperature is dominated by the assumed irradiation flux (see Figure 1).

With $\alpha_{\text{rd}} = 3 \times 10^{-4}$, the more numerous accretion outbursts for $f = 0.1$ case reduce the surface density compared with the results for $f = 0.01$ (Figure 3). However, the mass accretion rate and mass reservoirs are still comparable and within observational requirements. With a lower level of non-GI/MRI transport ($\alpha_{\text{rd}} = 3 \times 10^{-5}$), the surface density in the inner disc is higher and the Q -limited outer disc starts at a smaller radius of only $\sim 1 - 2$ AU, again similar to that of the quasi-steady model. The disc maintains an accretion rate of a few $\times 10^{-9} M_{\odot} \text{ yr}^{-1}$ during the T Tauri phase, accreting in total $\sim 0.01 M_{\odot}$ of mass onto the central star. As time goes on, mass is continually drawn from the Q -limited disk regions where $\Sigma \propto R^{-7/4}$; as this is steeper than the R^{-1} dependence for a steady constant α disk with $T \propto R^{-1/2}$ (Hartmann et al. 1998), the accretion rate $\dot{M} \propto \nu \Sigma$ must decrease with time. This decrease in our models is slow because of the long viscous times; it occurs somewhat faster in the low- α , $f = 0.01$ case because the Q -limited region becomes the mass reservoir sooner (see Figure 2).

6 DISCUSSION

The calculations of the previous section show that in the absence of rapid disc transport, protostellar collapse phase is likely to produce initially massive discs. Viscous or other transport timescales must be comparable to or shorter than typical low-mass protostellar lifetimes of ~ 0.4 Myr (§2) to avoid piling up mass in the disc; at scales of 10-100 AU, this requires viscous or equivalent α parameters $\sim 10^{-2}$ or larger (Equation 6; Kratter et al. 2008; Zhu et al. 2009). GI transport can redistribute mass effectively but by itself would still yield a massive disc. The effectiveness of wind transport during the protostellar phase is questionable, as the wind could be impeded or even quenched by the higher ram pressures of the infalling material. Dust in the infalling envelope might also extinct the ionizing stellar radiation needed for effective coupling of the magnetic field to the gas, which could also limit Hall effect transport. Finally, observations of protostellar accretion luminosities do not provide evidence for rapid accretion during this phase (see discussion in Hartmann et al. 2016).

The most direct evidence for large inner disc masses during or near the end of protostellar infall comes from study of the outbursting FU Ori objects (Hartmann & Kenyon 1996). FU Ori itself has a central gravitating mass (protostar) of $\sim 0.3 M_{\odot}$ accreting at a rate $\sim 2 \times 10^{-4} M_{\odot} \text{ yr}^{-1}$. FU Ori has been in a rapid accretion state for the ~ 80 yr duration of its outburst, and thus has accreted $\sim 0.02 M_{\odot}$ - about the same that equation 1 predicts is accreted on average by a $0.3 M_{\odot}$ star over its entire T Tauri disc lifetime. Analysis of the spectral energy distribution of FU Ori indicates that the rapid accretion region extends over $\sim 0.5 - 1$ AU in radius (Zhu et al. 2007); presumably the accreted mass has been drawn from this region. While FU Ori objects may not be typical of late stages of protostellar evolution, they do suggest that massive inner discs should be present in at least some objects at the start of the T Tauri phase.

If 1-Myr-old T Tauri inner discs have low masses, but

started out relatively massive at the end of infall, they must have had high accretion rates and/or photoevaporative rates at earlier times. The observational estimates discussed in §2 provide little or no evidence for sufficiently rapid early but post-infall accretion. Photoevaporative mass loss rates are uncertain, but if they are too large it would be difficult to explain those T Tauri systems whose disc lifetimes reach ~ 10 Myr.

Because the mass accretion in current disc wind models occurs only in thin layers in the upper disc, the magnetic transport is somewhat decoupled from the evolution of the central disc regions (but this may be modified by Hall effect: Béthune et al. 2017; Bai & Stone 2017). The Bai (2016) fiducial model adopts a residual hydrodynamic viscosity parameter of 2×10^{-4} . As this model has a surface density at 1 AU about five times smaller than that of the M-MMSN, the viscously-driven accretion is negligible compared with that of the wind; however, if the initial values of Σ were much larger, in better agreement with other solar nebula estimates (Weidenschilling 1977; Desch 2007), accretion due to viscous transport would have been comparable to that of the wind.

The models discussed here do not explain either the stellar mass- or time-dependence of accretion rates. Dullemond et al. (2006) attempted to explain the mass dependence as a result of initial disc sizes with viscous evolution. Lower-mass stars tend to have smaller discs (because they have smaller initial protostellar cores), and so they viscously evolve much faster, such that their accretion rates at a given age are much lower than those of larger stars, with larger discs and slower viscous depletion. Whether this explanation of the dependence of accretion on stellar mass can work with the much lower viscosities envisaged in this paper, or in concert with wind and/or Hall effect transport, is not clear.

Identifying the factors which determine disk lifetimes necessarily requires an explanation of the observed disk clearing timescales, which are much shorter than those expected from viscous evolution (the 'two-timescale' problem; Clarke et al. 2001). Models with photoevaporatively-driven winds (e.g., Clarke et al. 2001; Owen et al. 2011) can in principle explain the two-timescale behavior; the photoevaporative mass loss opens a gap in the disk, preventing replenishment of the inner disk gas that then drains onto the central star. (A giant planet could also open a gap to accomplish the same thing; Perez-Becker & Chiang 2011a,b.) However, with the low viscosities envisaged here, the inner disk clearing timescale would be too long. Possibly a disk wind working in concert with photoevaporation or planet gap formation could be a viable explanation. Alternatively, turbulence generated by planets in the inner disk (Fung & Chiang 2017) or by an outer giant planet (Bae et al. 2016) might be able to enhance transport sufficiently to clear the inner disk.

7 SUMMARY

We have shown that viscous disc models with $\alpha \gtrsim 10^{-4}$ can explain observed T Tauri mass accretion rates and lifetimes provided that mass surface densities are sufficiently large. The required values of Σ are not in conflict with any observational constraints nor do they imply gravitationally

unstable discs, and they are comparable to more recent estimates of solar and extrasolar nebula surface densities. The low viscosities are also consistent with observations limiting turbulence, providing favorable conditions for dust growth. Our considerations do not rule out the possible dominance of magnetic transport, but show that magnetic stresses may not be essential if hydrodynamic instabilities occur at low levels.

We acknowledge a helpful report from an anonymous referee. This work was supported in part by NASA grant NNX17AE31G and used computational resources and services provided by Advanced Research Computing at the University of Michigan, Ann Arbor.

REFERENCES

- Armitage P. J., Simon J. B., Martin R. G., 2013, *ApJ*, **778**, L14
 Bae J., Hartmann L., Zhu Z., Gammie C., 2013, *ApJ*, **764**, 141
 Bae J., Nelson R. P., Hartmann L., 2016, *ApJ*, **833**, 126
 Bae J., Zhu Z., Hartmann L., 2017, preprint, ([arXiv:1706.03066](https://arxiv.org/abs/1706.03066))
 Bai X.-N., 2014, *ApJ*, **791**, 137
 Bai X.-N., 2015, *ApJ*, **798**, 84
 Bai X.-N., 2016, *ApJ*, **821**, 80
 Bai X.-N., Stone J. M., 2013, *ApJ*, **769**, 76
 Bai X.-N., Stone J. M., 2017, *ApJ*, **836**, 46
 Balbus S. A., Hawley J. F., 1998, *Reviews of Modern Physics*, **70**, 1
 Béthune W., Lesur G., Ferreira J., 2017, *A&A*, **600**, A75
 Boley A. C., Mejía A. C., Durisen R. H., Cai K., Pickett M. K., D'Alessio P., 2006, *ApJ*, **651**, 517
 Cassen P., Moosman A., 1981, *Icarus*, **48**, 353
 Chiang E., Laughlin G., 2013, *MNRAS*, **431**, 3444
 Clarke C. J., Gendrin A., Sotomayor M., 2001, *MNRAS*, **328**, 485
 Cleeves L. I., Bergin E. A., Qi C., Adams F. C., Öberg K. I., 2015, *ApJ*, **799**, 204
 D'Alessio P., Calvet N., Hartmann L., 2001, *ApJ*, **553**, 321
 Desch S. J., 2007, *ApJ*, **671**, 878
 Dong R., Li S., Chiang E., Li H., 2017, *ApJ*, **843**, 127
 Dullemond C. P., Natta A., Testi L., 2006, *ApJ*, **645**, L69
 Espaillat C., et al., 2014, *Protostars and Planets VI*, pp 497–520
 Evans II N. J., et al., 2009, *ApJS*, **181**, 321
 Fedele D., van den Ancker M. E., Henning T., Jayawardhana R., Oliveira J. M., 2010, *A&A*, **510**, A72
 Ferreira J., Pelletier G., 1993, *A&A*, **276**, 625
 Ferreira J., Dougados C., Cabrit S., 2006, *A&A*, **453**, 785
 Flaherty K. M., Hughes A. M., Rosenfeld K. A., Andrews S. M., Chiang E., Simon J. B., Kerzner S., Wilner D. J., 2015, *ApJ*, **813**, 99
 Fromang S., Lesur G., 2017, preprint, ([arXiv:1705.03319](https://arxiv.org/abs/1705.03319))
 Fung J., Chiang E., 2017, *ApJ*, **839**, 100
 Furlan E., et al., 2006, *ApJS*, **165**, 568
 Gammie C. F., 1996, *ApJ*, **457**, 355
 Gressel O., Turner N. J., Nelson R. P., McNally C. P., 2015, *ApJ*, **801**, 84
 Griv E., 2006, *MNRAS*, **365**, 1007
 Guilet J., Ogilvie G. I., 2014, *MNRAS*, **441**, 852
 Hartmann L., Kenyon S. J., 1996, *ARA&A*, **34**, 207
 Hartmann L., Calvet N., Gullbring E., D'Alessio P., 1998, *ApJ*, **495**, 385
 Hartmann L., D'Alessio P., Calvet N., Muzerolle J., 2006, *ApJ*, **648**, 484
 Hartmann L., Herczeg G., Calvet N., 2016, *ARA&A*, **54**, 135
 Hayashi C., 1981, *Progress of Theoretical Physics Supplement*, **70**, 35
 Hernández J., et al., 2007, *ApJ*, **662**, 1067
 Hubeny I., 1990, *ApJ*, **351**, 632

- Kenyon S. J., Hartmann L., 1995, *ApJS*, **101**, 117
- Klahr H., Hubbard A., 2014, *ApJ*, **788**, 21
- Königl A., 1989, *ApJ*, **342**, 208
- Kratter K. M., Matzner C. D., Krumholz M. R., 2008, *ApJ*, **681**, 375
- Lesur G. R. J., Latter H., 2016, *MNRAS*, **462**, 4549
- Lesur G., Kunz M. W., Fromang S., 2014, *A&A*, **566**, A56
- Lin M.-K., Youdin A. N., 2015, *ApJ*, **811**, 17
- Lodato G., Scardoni C. E., Manara C. F., Testi L., 2017, preprint, ([arXiv:1708.09467](https://arxiv.org/abs/1708.09467))
- Marcus P. S., Pei S., Jiang C.-H., Barranco J. A., Hassanzadeh P., Lecoanet D., 2015, *ApJ*, **808**, 87
- Masson J., Chabrier G., Hennebelle P., Vaytet N., Commerçon B., 2016, *A&A*, **587**, A32
- Nelson R. P., Gressel O., Umurhan O. M., 2013, *MNRAS*, **435**, 2610
- Okuzumi S., Takeuchi T., Muto T., 2014, *ApJ*, **785**, 127
- Owen J. E., Ercolano B., Clarke C. J., 2011, *MNRAS*, **412**, 13
- Pascucci I., et al., 2011, *ApJ*, **736**, 13
- Perez-Becker D., Chiang E., 2011a, *ApJ*, **727**, 2
- Perez-Becker D., Chiang E., 2011b, *ApJ*, **735**, 8
- Pudritz R. E., Norman C. A., 1983, *ApJ*, **274**, 677
- Rafikov R. R., 2017, *ApJ*, **837**, 163
- Rigliaco E., Pascucci I., Gorti U., Edwards S., Hollenbach D., 2013, *ApJ*, **772**, 60
- Salmeron R., Wardle M., 2008, *MNRAS*, **388**, 1223
- Simon J. B., Lesur G., Kunz M. W., Armitage P. J., 2015, *MNRAS*, **454**, 1117
- Simon M. N., Pascucci I., Edwards S., Feng W., Gorti U., Hollenbach D., Rigliaco E., Keane J. T., 2016, *ApJ*, **831**, 169
- Tazzari M., et al., 2016, *A&A*, **588**, A53
- Tazzari M., et al., 2017, preprint, ([arXiv:1707.01499](https://arxiv.org/abs/1707.01499))
- Terebey S., Shu F. H., Cassen P., 1984, *ApJ*, **286**, 529
- Urpín V., 2003, *A&A*, **404**, 397
- Weidenschilling S. J., 1977, *Ap&SS*, **51**, 153
- Williams J. P., Best W. M. J., 2014, *ApJ*, **788**, 59
- Williams J. P., Cieza L. A., 2011, *ARA&A*, **49**, 67
- Zhu Z., Baruteau C., 2016, *MNRAS*, **458**, 3918
- Zhu Z., Hartmann L., Calvet N., Hernandez J., Muzerolle J., Tan-nirkulam A.-K., 2007, *ApJ*, **669**, 483
- Zhu Z., Hartmann L., Gammie C., 2009, *ApJ*, **694**, 1045
- Zhu Z., Hartmann L., Gammie C., 2010, *ApJ*, **713**, 1143